# Inviscid Analysis of a Dual Mode Scramjet Inlet

Yeu-Chuan Hsia,* Benjamin J. Gross,† and J. Paul Ortwerth‡
*Rockwell International Corporation, Canoga Park, California 91303*

**A three-dimensional inviscid flow computation was made on a dual mode scramjet inlet model that had been tested in the wind tunnels. An Euler solver based on a high accuracy total variation diminishing scheme was used to carry out the analysis. The objective was to establish three-dimensional scramjet inlet computational fluid dynamics capability and to evaluate the applicability of Euler solutions for inlet performance calculation. The computations were made for freestream Mach numbers 2 and 5. A postprocessor was developed to calculate the inlet performance. Comparison between computed and available test data showed the Euler analysis was able to predict the trend of the inlet performance and provide insight of the flowfield.**

## I. Introduction

SUPERSONIC combustion ramjet (or scramjet) is one of the candidate cycles for hypersonic propulsion. The development and design of a scramjet engine require a data base not yet available. Because of the high speed and high altitude of hypersonic flight, ground test facilities cannot simulate the full range and scope of the actual flight regime. Computational fluid dynamics (CFD) has been a promising method for extrapolating the test to the flight conditions. As an initial effort to establish the CFD capability of scramjet design, an inviscid simulation was carred out on the inlet. A dual mode scramjet inlet, which had been tested in wind tunnels,[1,2] was chosen as a design validation case.

The original inlet was proposed to operate in both ramjet and scramjet modes. It is a fixed-geometry, side-wall compression design. The side walls look like two spearheads. An isometric view of the model is shown in Fig. 1 and its dimensions in Fig. 2. A Cartesian coordinate system is used with the $X$ axis in the streamwise direction and the $Y$ and $Z$ axes in the cross plane. The inlet is 19 in. long including a 2.815-in. constant area throat section. The spearhead has an 8-deg included angle in the $X$-$Y$ plane and a 16.78-deg half-angle in the $X$-$Z$ plane. The cross sections of the flow path are rectangular. The width and height of the rectangles vary with the $X$ axis. The inlet frontal projection is a hexagon, having an area of 15.72 in.$^2$. The cross-sectional area of the throat is $6.093 \times 0.5$ in.$^2$, resulting in a contraction ratio of 5.16.

The test was made in the 40-in. supersonic and 50-in. hypersonic tunnels of the von Kármán Gas Dynamics Facility, Arnold Engineering Development Center, and completed in October 1966.[1,2] The Mach number range tested was from 2 to 10. The test Reynolds number per foot varied from $1.04 \times 10^6$ at $M_\infty = 10$ to $7.72 \times 10^6$ at $M_\infty = 3$. Test data obtained were the internal surface pressure distribution, pressure recovery, capture mass flow, and throat flow profiles.

The CFD Euler analysis reported here was made in October 1986. The Euler code was chosen instead of Navier-Stokes code to carry out the analysis because of the cost and the maturity of the code, as well as the available computer size and speed. Because of the time constraint and limited funding, only two Mach numbers (2 and 5) were computed. The computation was made on a Cray X/MP-14 computer. The CPU time used was about 3 h for Mach 2 and 1.5 h for Mach 5. A postprocessor was developed to calculate the numerically simulated inlet performance parameters from the converged Euler solution.

Presented as Paper 89-2681 at the AIAA/ASME/SAE/ASEE 25th Joint Propulsion Conference, Monterey, CA, July 10-12, 1989; received Oct. 30, 1989; revision received April 14, 1990. 

*Member, Technical Staff, Rocketdyne Division. Member AIAA.
†Member, Technical Staff, Rocketdyne Division.
‡Chief Scientist, Rocketdyne Division.

## II. Numerical Analysis

### A. CFD Code

A time-dependent, three-dimensional Euler solver[3] was used to carry out the computation. The solver makes use of the total variation diminishing (TVD) scheme, which is able to capture strong discontinuities (or shock waves) without spurious oscillations. This computer code solves the conservation-law-form Euler equations based on a finite-volume approach. The code has a multizone capability that allows computation of very complex geometries.[4]

### B. Grid System

The inlet configuration is symmetric about the $X$-$Y$ and $X$-$Z$ planes. For zero angle of attack and yaw, double symmetry can be assumed and only a quarter of the flowfield needs to be modeled. Spillage is an important part of inlet operation. In order to compute the spillage flow properly, the external flow region is also gridded. Thus, a far-field boundary condition can be applied. Figure 3 shows the zonal arrangement at two different types of cross sections. A total of five zones were used. Zone 1 modeled the region inside the inlet. Zones 2 to 5 covered the external flow region.

The actual grids on central $X$-$Y$ and $X$-$Z$ planes are shown in Figs. 4a and 4b, respectively. Zone 1 extended from the tip of the spearhead side wall to the end of the throat section ($X = 19.0$). Zones 2 to 5 extended to slightly downstream of

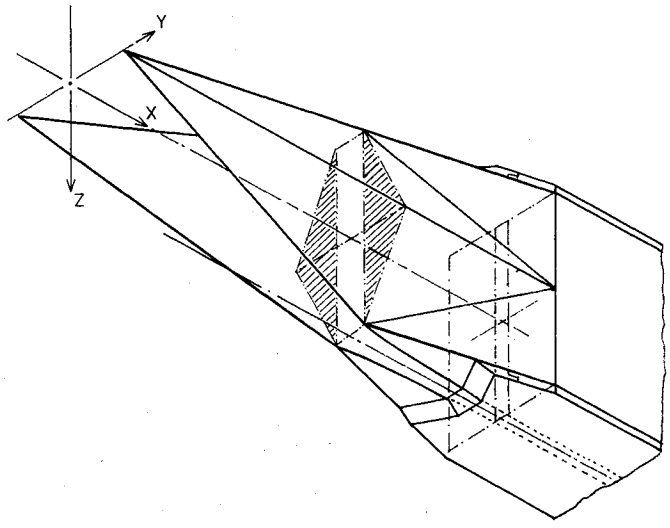


**Fig. 1 Isometric view of the inlet model with Cartesian coordinates.**

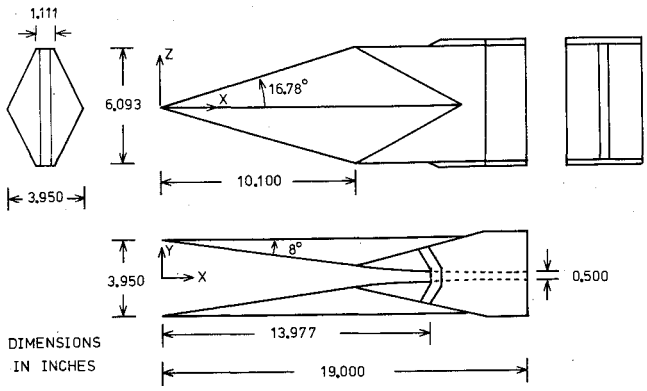


Fig. 2 Model dimensions and coordinates.

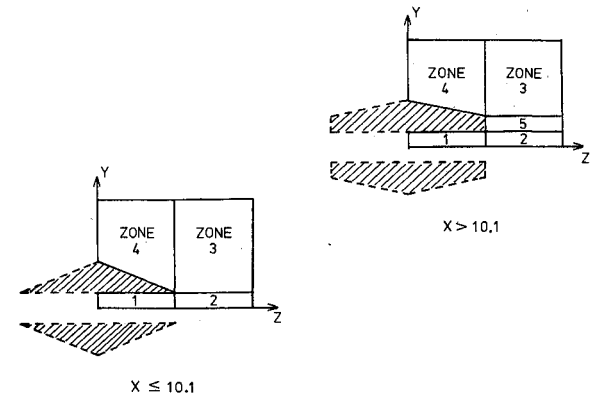


Fig. 3 Arrangement of the five-zone grid system at two $X$ locations.

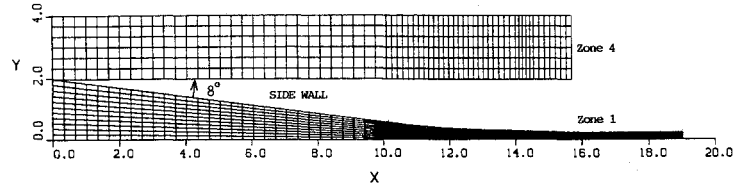


Fig. 4a Zones 1 and 4 grids in $X$-$Y$ plane.

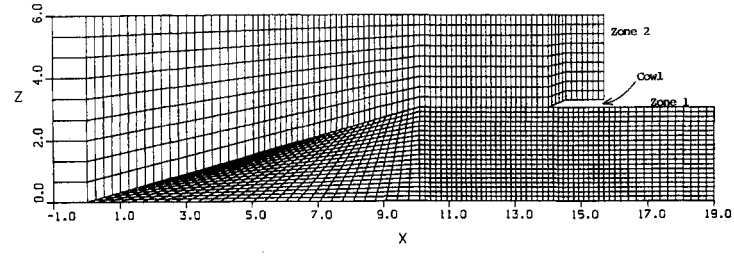


Fig. 4b Zones 1 and 2 grids in $X$-$Z$ plane.

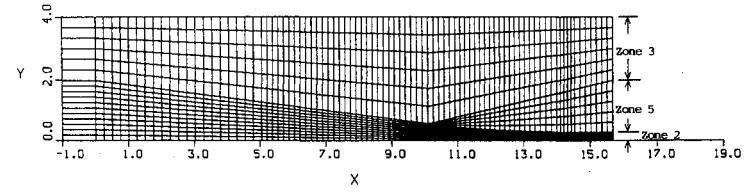


Fig. 4c Zones 2, 3, and 5 grids parallel to $X$-$Y$ plane.

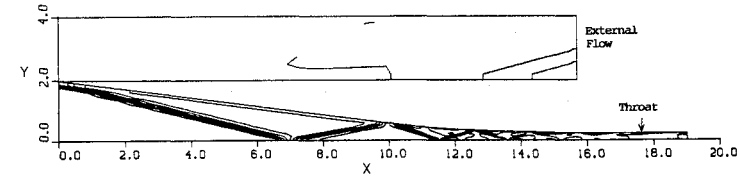


Fig. 5a Mach contours in $X$-$Y$ plane of $M_\infty = 5.0$.

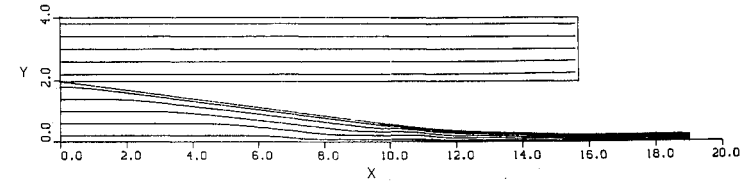


Fig. 5b Streamlines in $X$-$Y$ plane of $M_\infty = 5.0$.

the cowl leading edge. The exact thickness of the cowl was modeled (Fig. 4b). Figure 4c shows the projection of the grids in zones 2, 3, and 5 on the $X$-$Y$ plane. The grid points at zonal boundaries were matched between neighboring zones so that the interzonal boundary condition could be implemented easily. Because the Euler code required parallelepiped cells (or quadrilateral cell faces), the grids in the triangular shape region in zone 1 (see Fig. 4b) were generated by treating the leading edge as two sides of a quadrilateral. In zone 5, the cell faces of the first plane (see Fig. 4c, at $X = 10.1$) degenerated to a line, i.e., zero area.

### C. Boundary Conditions

The interzonal boundary condition (b.c.), which used a method consistent with the interior cells, was applied at all zonal connections. A symmetry b.c. was used on the $Y = 0.0$ and $Z = 0.0$ planes. A free slip surface tangency b.c. was used on the solid surfaces. A freestream b.c. was applied at inflow and far-field boundaries. A zero-gradient extrapolation b.c. was used at the flow exit planes. Zero fluxes were imposed on the degenerated cell faces as the boundary condition.

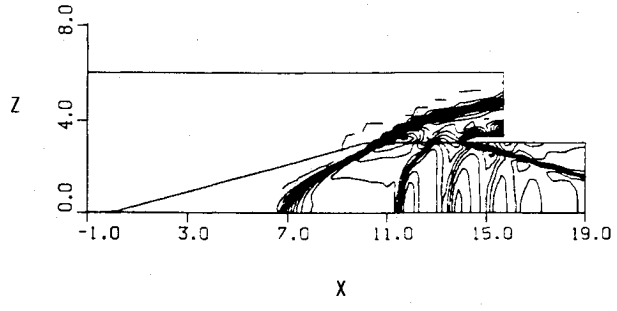


**Fig. 6a Mach contours in $X$-$Z$ plane of $M_\infty = 5.0$.**

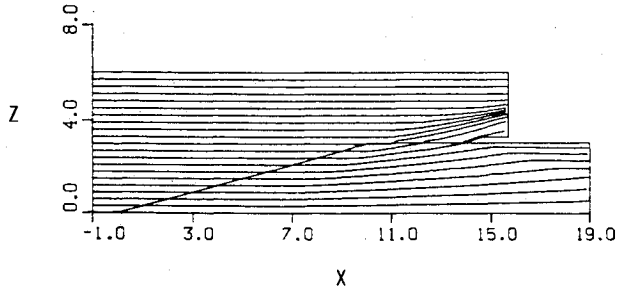


**Fig. 6b Streamlines in $X$-$Z$ plane of $M_\infty = 5.0$.**

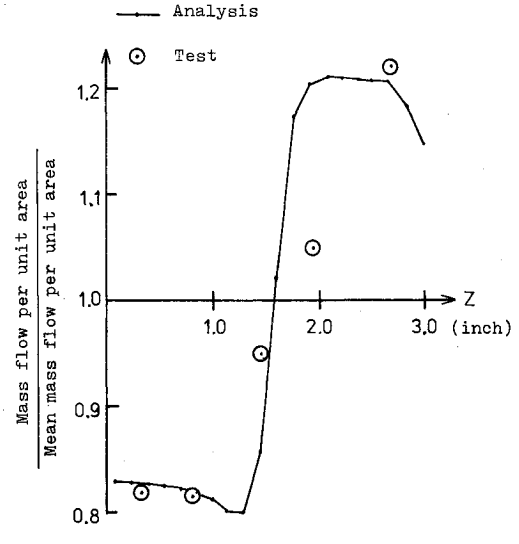


**Fig. 7 Normalized mass flow rate per unit area on $Z$ axis in the throat for $M_\infty = 5.0$.**

### D. Flowfield Results

Computations were done by initializing the flowfield with freestream conditions and then iterating in time until a converged solution was obtained. The criterion for convergence was that the net mass flux going into or out of the inlet control volume is less than 0.1% of the inflow mass flux. Solutions at both Mach 2 and 5 are presented here. The solutions obtained were fully three-dimensional but only those plots in the symmetry (i.e., central $X$-$Y$ and $X$-$Z$) planes are shown here due to graphics limitations. The solutions are presented using Mach number contours and streamlines. Normalized mass flow rate along the $Z$ axis in the throat is presented with available test data.

*1. $M_\infty = 5.0$*

Figures 5 and 6 represent Mach 5 solutions. The freestream flow is from left to right parallel to the $X$ axis. In Fig. 5a, Mach contours in the central $X$-$Y$ plane for the upper half of the inlet are shown. The clustered contours indicate shock waves. The shock-wave angle at the tip is about 15.8 deg, which is 1.8 deg less than that of a corresponding two-dimensional wedge. This is because the flow expands in the other dimension (i.e., parallel to $X$-$Z$ plane) and spills out of the inlet. The flow behind the oblique shock has a higher velocity than the corresponding wedge flow. A shock train extends all the way into the inlet throat. Five shock bounces on the side wall can be identified. The flowfield stays supersonic all the way into the throat. The mean Mach number in the throat is 2.97 (calculated using the method described in Sec. III.B). In the external flow region little gradient is seen, indicating that the effect of the outer boundary on the flowfield is negligible. This can be observed from the streamlines shown in Fig. 5b. Inside the inlet, the streamlines indicate that the flow gets contracted into the throat and the flow turns according to the oblique shock locations. In the central $X$-$Y$ plane, the internal and external flow regions are not connected. However, the inlet flow is allowed to spill in the dimension parallel to $X$-$Z$ plane.

Figures 6a and 6b show the flow in the central $X$-$Z$ plane. It can be observed that the inlet flow turns after the first oblique shock and bends a little bit more after the second shock. Part of the flow is therefore spilled out. The rest of the flow is intercepted by the cowl and then turned back into the throat, creating an oblique shock. As a result, most of the flow mass is near the cowl side.

In Fig. 7, the normalized mass flow per unit area is plotted along the throat centerline ($Y = 0$) on the positive $Z$ axis. The test results are included in the plot for comparison. Both the minimum and maximum flow rates are very close to the test data. The gradient in the middle is caused by the shock from the cowl. The computed shock location, at approximately $Z = 1.6$ in., agrees very well with the test. The test data seem to show a gradient less steep than the CFD solution. The experimental data are too sparse to compare the detailed profile of the analysis.

*2. $M_\infty = 2.0$*

Mach 2 inlet flow is quite different from that of Mach 5. In Fig. 8a, the contour lines started from the tip to the centerline indicate a weak oblique shock. The shock-wave angle at the tip is about 30 deg, while that of a corresponding two-dimensional wedge is 37 deg. The reduced shock angle in the inlet is mainly due to flow spillage. After two bounces on the compression wall, the oblique shock is terminated. A normal shock is formed at about $X = 8.8$ in. (Figs. 8a and 9a). This indicates that the inlet is at the unstart condition. Behind the normal shock, the flow is subsonic and expands in $X$-$Z$ dimension. Some of it is spilled out of the inlet (see Fig. 9b). This allows the inlet flow to accelerate back to supersonic. When

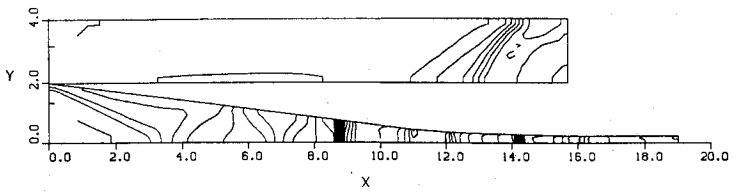


Fig. 8a Mach contours in $X$-$Y$ plane of $M_\infty = 2.0$.

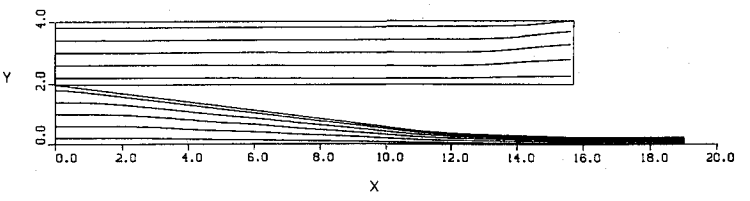


Fig. 8b Streamlines in $X$-$Y$ plane of $M_\infty = 2.0$.

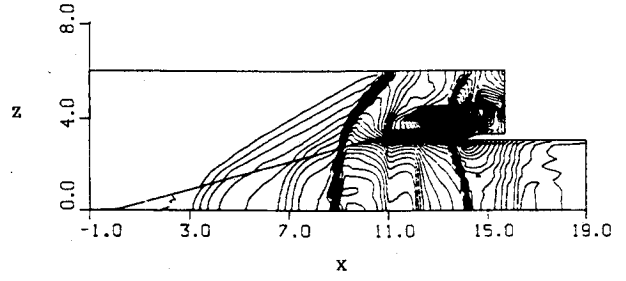


Fig. 9a Mach contours in $X$-$Z$ plane of $M_\infty = 2.0$.

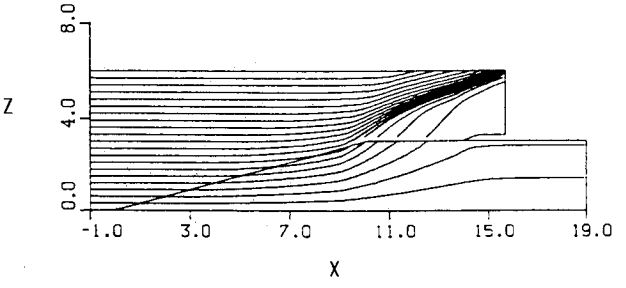


Fig. 9b Streamlines in $X$-$Z$ plane of $M_\infty = 2.0$.

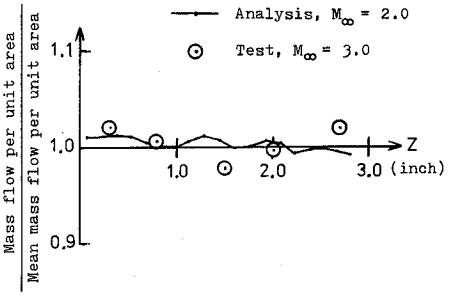


Fig. 10 Normalized mass flow rate per unit area on $Z$ axis in the throat for $M_\infty = 2.0$.

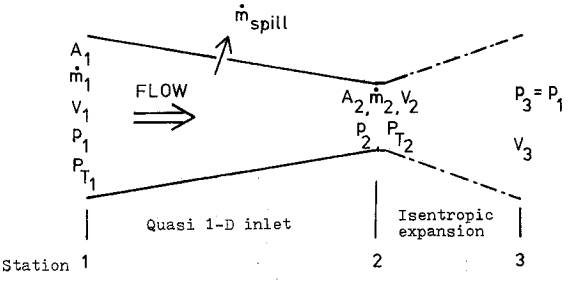


Fig. 11 Nomenclatures for inlet performance calculation.

this supersonic flow reaches the cowl, a detached shock is formed in front of the cowl leading edge. The shock becomes a normal shock on the inlet centerline at about $X = 14.0$ in. The flow downstream of this second normal shock becomes a converging subsonic flow, which accelerates and reaches a mean Mach number of 1.13 at the throat (computed by the method in Sec. III.B). This result may seem to contradict the fact that a normal shock is unstable in a convergent duct. The shock does stay there because it is detached from the cowl and therefore not totally inside the duct. The gap between the shock and cowl allows more spillage.

Because of the large spillage, the outer boundaries of the computational domain were found to be not far enough to apply the freestream b.c. Hence, the exit flow b.c. was applied for final results. In Figs. 8 and 9, no reflection from the outer boundaries can be observed and the effect of outer boundary on the inlet flow is expected to be minimal.

In Fig. 10, the normalized throat mass flow rate along the throat centerline for Mach 2 is shown. Unfortunately, no corresponding test data are available. Since the inlet is unstarted for both Mach 2 and 3 in the test, the Mach 3 data are included here as a qualitative guide. The relatively flat profile shown in Fig. 10 indicates that the flow is fairly uniform and that no shock wave exists in the throat.

## III. Performance Calculation

### A. Definitions for Quasi-One-Dimensional Inlet

Inlet performance is often characterized by the air capture ratio (ACR), pressure recovery (PR), and kinetic energy efficiency ($\eta_{ke}$). For a quasi-one-dimensional inlet (Fig. 11), the performance can be defined as follows:

$$\mathrm{ACR} = \frac{\dot{m}_2}{\dot{m}_1} = \frac{\rho_2 V_2 A_2}{\rho_1 V_1 A_1} \tag{1}$$

$$\mathrm{PR} = \frac{P_{T_2}}{P_{T_1}} \tag{2}$$

$$\eta_{ke} = \frac{V_3^2}{V_1^2} \tag{3}$$

where $\dot{m}$ is the mass flow rate, $\rho$ the density, $V$ the velocity, $A$ the cross-sectional area, and $P_T$ the total pressure. The subscripts denote the station. The velocity $V_3$ is the velocity that the flow in the throat (station 2) would obtain if it were isentropically expanded to the inflow pressure (at station 1).

### B. Definitions for Three-Dimensional Inlet

For the kind of inlet in which the flow is three-dimensional, integral or mean properties have to be used. The mass flow

rate is the integral of the product of density and velocity over the cross-sectional area, i.e.,

$$\dot{m} = \int_A \rho V \, dA$$

In the case of discrete solutions from numerical analysis, the mass flow rate can be found as

$$\dot{m} = \sum_{i=1}^{n} \rho_i V_i A_i$$

where $n$ is the total number of computational cells at a station. The air capture ratio is then calculated using Eq. (1).

The pressure recovery for the three-dimensional inlet is also defined by Eq. (2) except that the total pressures are substituted by mean total pressures. The mean total pressure is found from a one-dimensional flow having the same stream thrust $F$ and mass flow rate as the three-dimensional flow, i.e., a mass and momentum equivalent one-dimensional flow. The definition of the stream thrust is

$$F = \int_A (p + \rho V^2) \, dA = \sum_{i=1}^{n} (p_i + \rho_i V_i^2) A_i$$

where $p$ is the static pressure. For this equivalent one-dimensional flow, the mass and momentum equations have to be satisfied at each station, i.e.,

$$\dot{m} = \bar{\rho} \bar{V} A \tag{4}$$

$$F = (\bar{p} + \bar{\rho} \bar{V}^2) A \tag{5}$$

where $\bar{p}$, $\bar{\rho}$, and $\bar{V}$ are the pressure, density, and velocity of the one-dimensional flow.

For a perfect gas, $\bar{V}$ is equal to $\bar{M} (\gamma \bar{p}/\bar{\rho})^{1/2}$, where $\bar{M}$ is the Mach number of the one-dimensional flow. Equations (4) and (5) can then be reduced to a quadratic equation

$$\frac{\dot{m}}{F} = \frac{\bar{M} (\gamma \bar{\rho}/\bar{p})^{1/2}}{1 + \gamma \bar{M}^2}$$

Assuming adiabatic flow, $\bar{p}$ and $\bar{\rho}$ are functions of $\bar{M}$ only. Thus, the only unknown in the above equation is $\bar{M}$.

For most cases, two solutions for $\bar{M}$ can be obtained, one supersonic and the other subsonic. The subsonic solution at the throat location is equivalent to the flow behind a normal shock if the flow in the throat is supersonic. With these mean Mach numbers, mean total pressures can be calculated:

$$\bar{P}_T = \bar{p} \left( 1 + \frac{\gamma - 1}{2} \bar{M}^2 \right)^{\gamma/(\gamma - 1)}$$

Thus, the pressure recovery can be found from Eq. (2).

If we assume that the flow is adiabatic, the total enthalpy is conserved, i.e.,

$$\bar{h}_1 + \frac{\bar{V}_1^2}{2} = \bar{h}_3 + \frac{\bar{V}_3^2}{2} \tag{6}$$

The enthalpy is calculated from $\bar{p}$ and $\bar{\rho}$:

$$\bar{h} = \frac{\gamma}{\gamma - 1} \frac{\bar{p}}{\bar{\rho}}$$

Substituting $\bar{V}_3$ of Eq. (6) in Eq. (3), the kinetic energy efficiency can be computed:

$$\eta_{ke} = \frac{2(\bar{h}_1 - \bar{h}_3)}{\bar{V}_1^2} + 1$$

where

$$\bar{V}_1 = \bar{M}_1 \left( \frac{\gamma \bar{p}_1}{\bar{\rho}_1} \right)^{1/2}$$

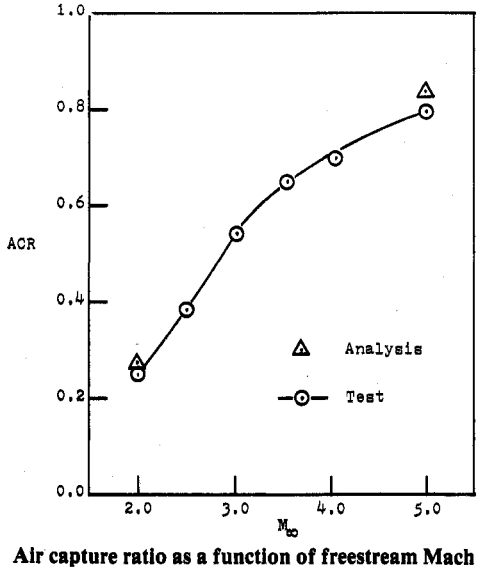


**Fig. 12a Air capture ratio as a function of freestream Mach number.**

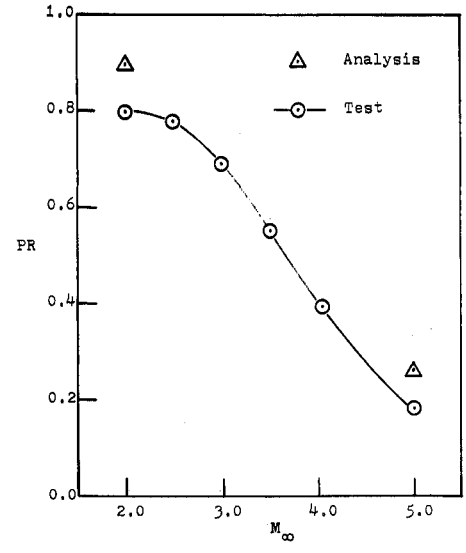


**Fig. 12b Pressure recovery as a function of freestream Mach number.**

### C. Comparison of Computed Performance and Test Data

A postprocessor based on the definitions and method described above was coded. Air capture ratio, pressure recovery, and kinetic energy efficiency were computed from the Euler solutions. Figures 12a and 12b show the air capture ratio and pressure recovery as functions of Mach number for both numerical and test results. Kinetic energy efficiency was not available from the test reports.

The air capture ratio from the test shows a monotonic increase with respect to Mach number (see Fig. 12a), which is typical of a fixed-geometry scramjet inlet. This is because at lower Mach number the flow is more difficult to compress through a large contraction. Therefore, a larger percentage of the flow is spilled out at lower Mach numbers. The computation shows the same trend as the test data. The computed values are 0.27 for Mach 2 and 0.84 for Mach 5, compared with 0.25 and 0.79, respectively, from test. The mass capture is consistently well predicted. The small discrepancy may be due to lack of boundary-layer displacement effects in the Euler analysis. The boundary layers in the wind-tunnel model created a blockage effect that resulted in less air capture.

**Table 1 Computed inlet performance data**

| | | $\bar{M}_2 < 1$ | | $\bar{M}_2 > 1$ | |
|---|---|---|---|---|---|
| $M_\infty$ | ACR | PR | $\eta_{ke}$ | PR | $\eta_{ke}$ |
| 2.0 | 0.274 (0.25) | 0.924 (0.80) | 0.971 | 0.926 | 0.972 |
| 5.0 | 0.838 (0.79) | 0.262 (0.19) | 0.907 | 0.804 | 0.987 |

Figure 12b shows the pressure recovery vs Mach number for both numerical and test results. The test data were taken when there was a normal shock in the throat during a throttling process. To be consistent, the numerical data plotted are based on the subsonic solution described in the previous subsection. The pressure recovery shows a monotonic decrease with respect to Mach number. The large loss in total pressure at high Mach numbers is due to the large entropy increase across strong shocks. The computed pressure recovery is 0.92 for Mach 2 and 0.26 for Mach 5, compared to 0.80 and 0.19, respectively, from test. Again, the trends of the variation agree. The pressure recovery is overpredicted. This can be explained by the existence of boundary layers in the wind-tunnel model. The effect of viscosity on the total pressure is twofold. First, the displacement effect of the boundary layer increases the effective side wall compression angle which produces larger shock-wave angles and hence greater shock losses. Second, the viscous losses inside the inlet throat reduce the normal shock recovery and overall inlet pressure recovery.

For the sake of completeness and documentation, the computed inlet performance data are listed in Table 1. The available test data are included in parentheses for reference.

## IV. Conclusions

The flowfield of a dual mode scramjet inlet has been analyzed using a three-dimensional Euler code. The multizone capability together with the finite-volume method of the code allowed modeling of complex geometry with mixed internal and external flowfields. The shock waves were cleanly captured and the shock location in the throat agreed with the test data. The code was able to analyze not only the normal operation but also the unstart condition.

A postprocessor was developed to calculate the inlet performance that included air capture ratio, pressure recovery, kinetic energy efficiency, etc. Compared to the available test data, the numerical results showed good agreement on the air capture ratio and the trend of the pressure recovery. The overprediction of the pressure recovery was believed to be resulted from the inviscid assumption of the Euler equations.

The results reported here are only part of the information that can be obtained from the CFD solution. Other information, such as flow uniformity, lift and drag, shock strength, aerodynamic loads on structures, etc., can also be extracted. This Euler solver, incorporated with the postprocessor for inlet performance calculation, can serve as a design tool for a three-dimensional scramjet inlet.

## Acknowledgments

This work was supported under a Rocketdyne Independent Research and Development project. The Euler code used in this study was developed by the Rockwell International Science Center. The authors would like to thank Sukumar Chakravarthy, Dale Ota, and Kuo-Yen Szema of the Rockwell Science Center for their valuable advice and discussions on using the computer code. The computation was carried out on the Rockwell International Cray X/MP-14 computer. The sketch in Fig. 1 was traced from a blueprint expertly drawn by Larry Russell of Rocketdyne.

## References

[1]Baer, A. L., and Lucas, E. J., "Wind-Tunnel Tests of Dual Mode Scramjet Inlet Configurations at Mach Numbers from 2.5 to 6," Arnold Engineering Development Center, AEDC-TR-67-60, Tullahoma, TN, April 1967.

[2]Baer, A. L., "Wind-Tunnel Tests of a Marquardt Dual Mode Scramjet Inlet Model at Mach Numbers from 2 to 10," Arnold Engineering Development Center, AEDC-TR-67-105, Tullahoma, TN, July 1967.

[3]Chakravarthy, S. R., and Szema, K. Y., "An Euler Solver for Three Dimensional Supersonic Flows with Subsonic Pockets," *Journal of Aircraft*, Vol. 24, No. 2, 1987, pp. 73–83.

[4]Chakravarthy, S. R., "The Versatility and Reliability of Euler Solvers Based on High-Accuracy TVD Formations," AIAA Paper 86-0243, Jan. 1986.